PHOTONICS Research

Ultra-flat dispersion in an integrated waveguide with five and six zero-dispersion wavelengths for mid-infrared photonics

YUHAO GUO,[1] ZEINAB JAFARI,[1,2] (iD) LIJUAN XU,[1,3] CHANGJING BAO,[4] PEICHENG LIAO,[4] GUIFANG LI,[5] ANURADHA M. AGARWAL,[6] LIONEL C. KIMERLING,[6] JURGEN MICHEL,[6] ALAN E. WILLNER,[4] AND LIN ZHANG[1,*]

[1]Key Laboratory of Opto-electronic Information Technical Science of Ministry of Education and Key Laboratory of Integrated Opto-electronic Technologies and Devices in Tianjin, School of Precision Instruments and Opto-electronics Engineering, Tianjin University, Tianjin 300072, China
[2]School of Computer and Electrical Engineering, Shiraz University, Shiraz, Fars, Iran
[3]School of Electronic Engineering, Tianjin University of Technology and Education, Tianjin 300222, China
[4]Department of Electrical Engineering, University of Southern California, Los Angeles, California 90089, USA
[5]College of Optics and Photonics, CREOL and FPCE, University of Central Florida, Orlando, Florida 32816, USA
[6]Department of Materials Science and Engineering, Massachusetts Institute of Technology, Cambridge, Massachusetts 02139, USA
*Corresponding author: lin_zhang@tju.edu.cn

We propose a new type of dispersion flattening technology, which can generate an ultra-flat group velocity dispersion profile with five and six zero-dispersion wavelengths (ZDWs). The dispersion value varies from −0.15 to 0.35 ps/(nm·km) from 4 to 8 μm, which to the best of our knowledge is the flattest one reported so far, and the dispersion flatness is improved by more than an order of magnitude. We explain the principle of producing six ZDWs. Mode distribution in this waveguide is made stable over a wide bandwidth. General guidelines to systematically control the dispersion value, sign, and slope are provided, and one can achieve the desired dispersion by properly adjusting the structural parameters. Fabrication tolerance of this waveguide is also examined. © 2019 Chinese Laser Press

https://doi.org/10.1364/PRJ.7.001279

1. INTRODUCTION

Chromatic dispersion is one of fundamental properties of optical waveguides, which not only plays a critical role in shaping the temporal waveform of an optical pulse but also acts together with nonlinearity to affect pulse spectral evolution [1]. In nonlinear parametric interactions of continuous waves at different frequencies, dispersion is important in determining phase-matching conditions [1]. Thus, dispersion engineering has been widely used for parametric oscillation/amplification, supercontinuum, and frequency comb generation [2–4]. These technologies are indispensable to build broadband or octave-spanning optical sources for spectroscopy, imaging, frequency metrology, and communication.

In general, one needs to control many aspects of dispersion properties: (i) sign (i.e., normal or anomalous), (ii) value, (iii) dispersion slope, (iv) the number of ZDWs, (v) bandwidth where the dispersion of interest is obtained, and (vi) dispersion flatness (defined as flat-dispersion bandwidth divided by dispersion variation). Specific for broadband nonlinear applications [2–4], dispersion flattening is critical in achieving broadband phase-matching and high conversion efficiency. Dispersion engineering has been shown as a key enabler for

two-octave frequency comb generation [5], three-octave supercontinuum generation [6], and octave-spanning amplification [7]. However, it is quite challenging to control multiple aspects of dispersion properties simultaneously in conventional optical waveguides. Dispersion naturally originates from materials and device structures and inevitably varies if one considers a large-enough bandwidth. In many cases, with multiple ZDWs, a dispersion profile tends to be bonded in a small variation range, and in this way the dispersion is made "flat".

In recent years, dispersion engineering with multiple ZDWs has been proposed in various types of optical devices, such as photonic crystal fibers [8–12] and integrated waveguides [13–26]. In fibers, saddle-shaped dispersion curves with three and four ZDWs can be obtained by complicated geometry profiles, as a result of balanced waveguide dispersion and material dispersion. In integrated waveguides, a high-index contrast and tight mode confinement cause strong waveguide dispersion, which is usually dominant over material dispersion [13]. Therefore, dispersion flattening with multiple ZDWs is obtained by inducing additional waveguide dispersion from new structures to compensate for existent material/waveguide dispersion. As an example, strip/slot hybrid silicon waveguides

over a large bandwidth have been proposed [14,15], and the general design guidelines of the nano-slot structures are also presented [17]. Different material combinations are proposed to achieve low and flat dispersion in single-slot and dual-slot waveguides [18,19,21,22]. Bilayer waveguides have been proposed to flatten dispersion with four ZDWs with the slot layer removed [24]. Compared to slot-assisted waveguides, these waveguides can be formed with a relatively low index contrast, making choices of materials more flexible and more fabrication-friendly.

Nevertheless, there are still some fundamental questions remaining unanswered. For example, how flat can a dispersion profile be? Is there an ultimate limit on the number of ZDWs? What is the maximum bandwidth for dispersion flattening?

These questions are important not only for deepening our understanding of dispersion engineering principle but also for practical applications. For example, middle infrared (mid-IR, from 2.5 to 20 μm, i.e., three octaves) is of particular interest recently [6,27–30], and on-chip mid-IR photonics [5,7,31–36] is intensively investigated. A research focus is to produce supercontinua [6,31–33] and broadband frequency combs [5,34,35] for spectroscopy/sensing and imaging applications [37,38]. In such a broad spectral region (three octaves), many conventional optical materials become absorptive, while some usable materials are mainly with high index [27], typically associated with strong waveguide dispersion. On the other hand, nonlinear photonics in deep mid-IR faces severe challenges [5], and these factors urge us to pursue dispersion flattening with multiple ZDWs as a promising technology for mid-IR applications. We list recent results in Table 1, including some works aiming to obtain low and flat dispersion in mid-IR using high-index materials such as Ge and Ge_xSi_{1-x} [5,33,39,40] for a comparison of dispersion-flattened waveguides in terms of dispersion flatness and the number of ZDWs.

In this work, we propose a new type of integrated waveguide, in which different material combinations can be used to realize dispersion flattening. An ultra-low and flat dispersion profile can be obtained over an octave-spanning bandwidth in mid-IR, with a total variation of 0.5 ps/(nm·km), which to the best of our knowledge is the flattest one reported so far. More importantly, we show how to produce five or even six ZDWs in the proposed waveguides with different material combinations, which demonstrates unprecedented capability and versatility of dispersion engineering in integrated photonic waveguides.

2. DISPERSION FLATTENING PRINCIPLE

For dispersion tailoring with multiple ZDWs, a natural and fundamental question would be how many ZDWs a waveguide can have. If possible, producing more ZDWs, as shown in Fig. 1(a), not only deepens our understanding on the principle of dispersion engineering but can also significantly extend the low-dispersion bandwidth, which is highly desirable for broadband nonlinear applications [5–7]. Since a nano-scale slot has been successfully used for inducing normal dispersion in the middle of dispersion bandwidth and two more ZDWs [14,15], one may think of adding another slot layer to produce more than four ZDWs, as shown in Fig. 1(b). Note that, in this way, the second slot has to be designed for a longer wavelength, in order to introduce another dip in the dispersion profile in Fig. 1(a). By properly adjusting structural parameters, one may in principle obtain a dispersion profile with two more ZDWs, compared to the slot-assisted waveguides in Refs. [14,15].

However, there is an obvious drawback of this waveguide, i.e., the mode will be continuously lifted up as wavelength increases [15], which may result in a small optical field overlap between two modes that are spectrally far apart. Then, this causes a significant reduction in the effective nonlinear interaction over an octave-spanning bandwidth and a decrease in nonlinear conversion efficiency. Therefore, it is preferred to keep the guided mode stable in the vertical direction, while engineering a dispersion profile. To this end, we introduce a slab beneath the waveguide core so that the guided mode extends to the slab more at a longer wavelength, as shown in Fig. 1(c). Note that we also coat the waveguide core with a low-index layer. Without it, the mode can be dragged down to the slab quickly as wavelength increases. Finally, the proposed waveguide is presented in Fig. 1(d). At short wavelengths, the guided mode is tightly confined in the lower layer of the inner trilayer waveguide as in Refs. [14,15], simply like a strip mode.

Table 1. Comparison of Dispersion-Flattened Waveguides in Recent Works

Year	Material	ZDWs	Dispersion [ps/(nm·km)]	λ (nm)	$\Delta\lambda$ (nm)	Flatness (nm² · km/ps)
2011 [14]	$Si_3N_4 + SiO_2$[a]	4	−32 to −11	1565–2100	535	25.48
2012 [15]	$Si + SiO_2$	4	−22 to +20	1435–2102	667	15.88
2012 [18]	$Si + Si–nc$	4	−24 to +22	1527–2625	1098	23.87
2012 [19]	$As_2S_3 + SiO_2$	4	−3 to +3	1685–2720	1035	172.50
2013 [21]	$Si + Si–nc$	4	−13 to +14	1810–2655	845	31.30
2015 [22]	$Si_3N_4 + SiO_2$	4	−1 to +1	1137–1949	682	341.00
2016 [24]	$TiO_2 + Si_3N_4$	4	−15.87 to +11.34	1520–2320	800	29.40
2016 [24]	$Si + GeSbSe$	4	−4.7 to +5.7	1660–3290	1630	156.73
2016 [39]	$Si_{1-x}Ge_x$	2	0 to +14	3000–8000	5000	357.14
2017 [40]	$Ge + Si$	2	0 to +59	3840–7920	4080	69.15
2018 [5]	$Ge + Si$	4	−16 to +32	3500–10,000	6500	135.42
2018 [33]	$Si_{0.6}Ge_{0.4} + Si$	2	0 to +19	4500–7700	3200	168.42
This work	$GeSbSe + GeSbS$	5	−0.15 to +0.35	4000–8000	4000	8000.00
	$Si + Al_2O_3 + Si_3N_4$	6	−3.6 to +5.1	2030–5030	3000	344.87

[a]The saddle-shaped dispersion curve in this paper can be moved to generate four ZDWs while keeping the dispersion flatness almost unchanged.
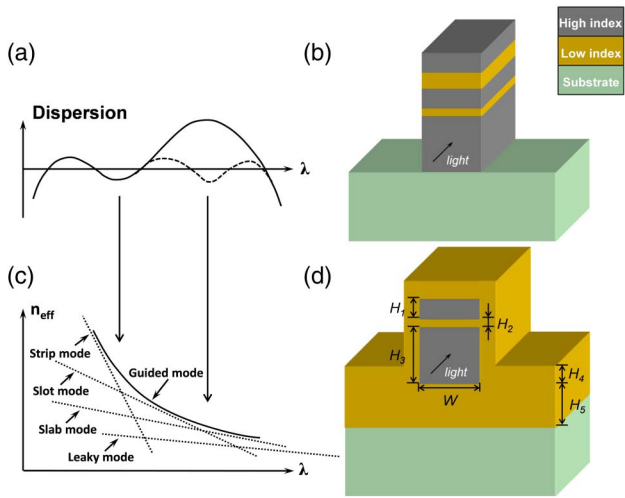
Fig. 1. Scheme for obtaining dispersion profile with more ZDWs. (a) The dispersion profile with another dip can introduce two more ZDWs. (b) The waveguide structure can generate the dispersion curve in (a), with one more slot layer added. (c) A slab beneath the waveguide core is introduced so that the guided mode extends to the slab more at a longer wavelength. (d) The proposed waveguide in this work.

As wavelength increases, the first mode transition occurs within the inner trilayer part assisted by a slot layer [15], generating a saddle-shaped dispersion profile. At longer wavelengths, the guided mode extends into both the coat and the slab. The mode experiences the second transition as in Ref. [24], and in this process the inner trilayer part together with the coat, as a whole, can be regarded as the waveguide core, and the mode shifts from it toward the slab as in a bilayer waveguide proposed in Ref. [24], which forms the second saddle-shaped dispersion. Finally, a low and flat dispersion with two more ZDWs can be obtained by choosing an appropriate parameter set.

3. RESULTS OF DISPERSION ENGINEERING

A. Proposed Dispersion-Flattened Waveguides

The waveguide can be formed by different combinations of materials, and here we show two cases (WG1 and WG2). In WG1, the materials are $Ge_{28}Sb_{12}Se_{60}$ (GeSbSe, $n \approx 2.6$)

and $Ge_{23}Sb_7S_{70}$ (GeSbS, $n \approx 2.2$), and the substrate is CaF_2. In WG2, the materials are Si ($n \approx 3.4$), Al_2O_3 ($n \approx 1.65$, slot), and Si_3N_4 ($n \approx 2$, coat and slab), and the substrate is air, which can be formed by partially wet-etching SiO_2 in an SOI wafer [41]. Different from WG1, the materials of the slot layer and the coat layer are not the same for WG2, which are Al_2O_3 and Si_3N_4 individually. All material dispersions are taken into account using Sellmeier equations [29,42–44]. We employ a full-vectorial mode solver to obtain the effective refractive index (n_{eff}) of the fundamental quasi-TM mode. The chromatic dispersion of the guided mode is expressed by

$$D = -\left(\frac{\lambda}{c}\right) \cdot \left(\frac{\partial^2 n_{eff}}{\partial \lambda^2}\right), \tag{1}$$

where λ is the wavelength, and c is the speed of light in vacuum.

For WG1, the parameters of the structure are $W = 2200$ nm, $H_1 = 720$ nm, $H_2 = 450$ nm, $H_3 = 2585$ nm, $H_4 = 720$ nm, and $H_5 = 2730$ nm. Figure 2(a) shows the dispersion of the guided mode. An ultra-low and flat dispersion profile can be obtained from 4 to 8 μm wavelengths. As clearly seen from the inset, the dispersion varies from –0.15 to 0.35 ps/(nm·km), with five ZDWs located at 3.98, 4.66, 5.42, 7.08, and 7.52 μm, respectively. We see from Table 1 that the dispersion flatness of this waveguide is quite high compared to previous works. Note that the anomalous dispersion at wavelengths beyond 8 μm is due to the material dispersion of CaF_2 substrate [43].

For WG2, the parameters of the structure are $W = 875$ nm, $H_1 = 247$ nm, $H_2 = 50$ nm, $H_3 = 650$ nm, $H_4 = 855$ nm, and $H_5 = 580$ nm. For the slot, the dispersion of the guided mode is presented in Fig. 2(b), and a low and flat dispersion with a change from –3.6 to 5.1 ps/(nm·km) can be obtained from 2.03 to 5.03 μm. Different from WG1, it is noted that there are six ZDWs generated by WG2, which are located at 2.12, 2.49 3.14, 3.78, 4.45, and 5.02 μm, respectively. In addition, the dispersion variation for WG2 is larger, due to a higher index contrast among waveguide materials [17]. Details of the dispersion profiles are shown in the insets of Fig. 2 individually for WG1 and WG2.

These two examples show flexibility of material choices in the proposed dispersion flattening technology. We note that, in terms of index contrast as a key parameter defined as refractive
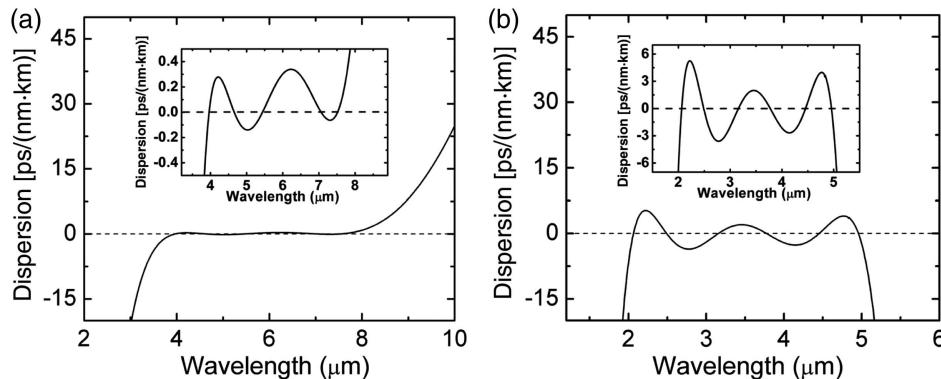

Fig. 2. Dispersion profiles of the guided mode over a wideband (a) for WG1 and (b) for WG2. Details of the dispersion are shown in the insets, individually.

index ratio [17], WG1 and WG2 have quite different index ratios. Also, in WG2, high and low refractive indices cover a larger range than those in WG1. This means that one can effectively tailor dispersion for more than 4 ZDWs with material combinations from a wide range of optical materials. In other words, the proposed dispersion engineering technique can serve as general methodology, instead of being found out with a special trick.

B. Mode Evolution in This Waveguide

The mode evolution in the proposed waveguide is illustrated in Fig. 3(a). At short wavelengths, the guided mode is tightly confined in the high-index layer of the inner trilayer waveguide, simply like a strip mode. As wavelength increases, the mode extends more into the slot (first mode transition) [15], generating a saddle-shaped dispersion profile. At longer wavelengths, the guided mode extends further into the coat and slab layers. In this transition, the slab and the waveguide structure above the slab form a "bilayer" waveguide as in Ref. [24] and produce the second dispersion dip. Note that, to explain in principle, we differentiate the two mode transitions as wavelength increases, but the two processes cannot be clearly separated. In fact, the mode stays quite stable in the vertical direction, instead of moving up and then down. Figure 3(a) shows the optical field distributions of the guided mode in WG1 at 4, 5, 6, 7, and 8 μm. We can see that the mode is well centered in the lower GeSbSe layer as wavelength increases.

C. Guidance for Dispersion Tailoring

For broadband or octave-spanning nonlinear applications, modal field overlap among far apart frequency components becomes an important issue, and low modal overlap can lead to a significant reduction of nonlinear conversion efficiency [45]. To verify the advantages of the proposed waveguide, we calculate the mode overlap factor [46] between different wavelengths for WG1. Here, we choose a mode located at 6 μm and obtain its mode overlap factors with other fundamental TM modes at 4, 5, 7, and 8 μm, as shown in Fig. 3(b), which
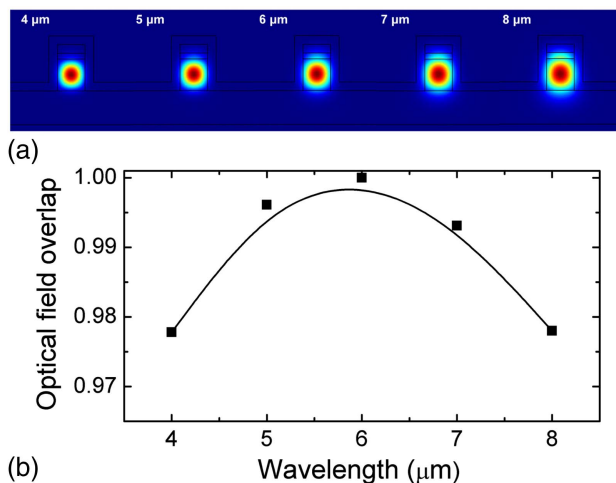

(a)

(b)

Fig. 3.   Mode evolution in this waveguide. (a) Optical field distributions of the quasi-fundamental-TM mode in WG1 at 4, 5, 6, 7, and 8 μm, respectively. (b) Normalized optical field overlaps of a fixed mode located at 6 μm with other modes at 4, 5, 7, and 8 μm.

are 0.9778, 0.9961, 0.9931, and 0.9780, respectively. This means that the influence of modal field mismatch is negligible in broadband nonlinear processes in the proposed waveguide.

Although flattened dispersion is needed in general for broadband nonlinear applications, a dispersion profile has to be optimized specifically for each application scenario [5–7]. The guidance for dispersion tailoring in the proposed waveguides to achieve the desired dispersion properties is presented in Fig. 4. Since WG2 has a dispersion profile not dominated by material dispersion at the long-wavelength end and also dispersion engineering is mainly about how to tailor waveguide dispersion, we take WG2 as an example to show how a dispersion profile can be shaped in different ways over a wavelength band more than one octave. We change each of the structural parameters around the values given for Fig. 2(b) by 1%–2% every time, while keeping the others fixed. As seen from Fig. 4(a), dispersion at long wavelengths is more sensitive to W and becomes more anomalous as W increases. Figure 4(b) shows that the dispersion profile rotates as we increase H_1 gradually, with a nearly zero value at around 3.5 μm, which is almost the center of the flat-dispersion band. Thus, one can modify the third-order dispersion, while keeping the average dispersion almost unchanged over a wide bandwidth. The influence of the slot layer on the total dispersion is illustrated in Fig. 4(c). In contrast with Fig. 4(b), dispersion at the central wavelength is more sensitive than at other wavelengths, producing a nearly symmetric dispersion profile over wide spectra as H_2 becomes larger. As we increase H_3, the dispersion profile is entirely moved up without a dramatic change in its shape and slope, which means that we can obtain the same flat-dispersion bandwidth with different signs. Figure 4(e) shows that H_4 has increasingly more influence on dispersion after ∼3 μm, due to the fact that more and more power extends to the coat layer as wavelength increases and the dispersion is changed to be normal with the increased H_4. Figure 4(f) presents that the slope of dispersion can be slightly tailored by modifying H_5, and dispersion is less sensitive to this parameter compared to others.

From above, it is outlined that a dispersion profile in the proposed waveguide can be rotated, as in Figs. 4(a), 4(b), 4(e), and 4(f), and moved up and down as in Fig. 4(d), while its shape can be modified as in Fig. 4(c). For a rotation of a dispersion profile, Figs. 4(a) and 4(e) represent a coarse tuning, and Fig. 4(f) shows a fine tuning, while Fig. 4(b) provides a different rotation center. It is important to emphasize that one may need to simultaneously vary more than one parameter to reach the goals of dispersion engineering listed in the introduction section. For example, by jointly varying H_2 and H_3 and keeping the others same, one can make both the second-order and third-order dispersion nearly zero from 3 to 4 μm. Generally speaking, the flexibility of dispersion tailoring in the proposed waveguide provides us with a valuable and significantly extended parameter space for waveguide properties, allowing manipulation of ultrashort optical pulses over an ultrabroadband spectral range by precisely controlling the timing of intra-pulse frequency components. This would greatly enrich broadband nonlinear phenomena, beyond what have been proposed in Refs. [5–7].
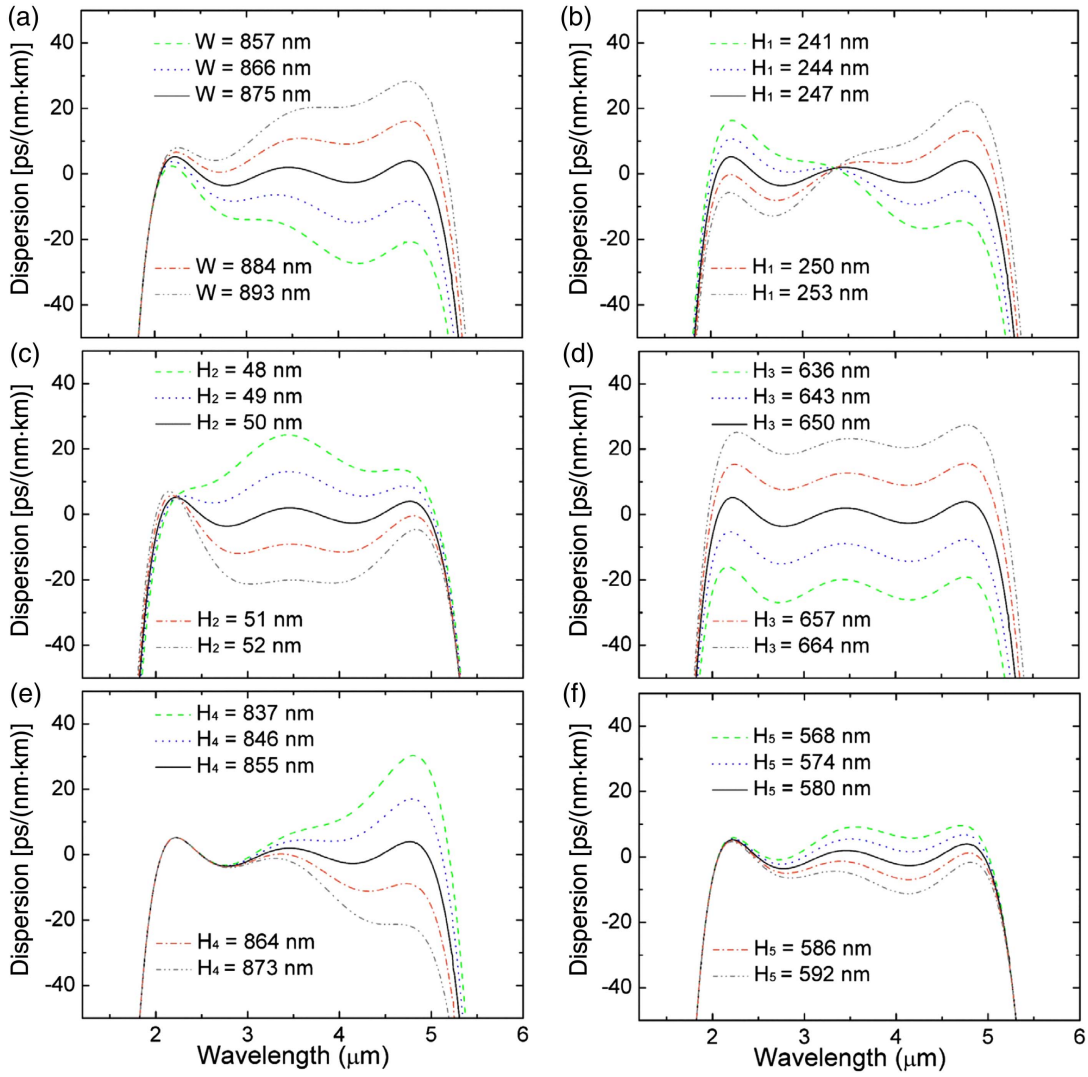
Fig. 4. Dispersion profiles for WG2 with different structural parameters changed around the optimal values. (a) Different W, (b) different H_1, (c) different H_2, (d) different H_3, (e) different H_4, and (f) different H_5.
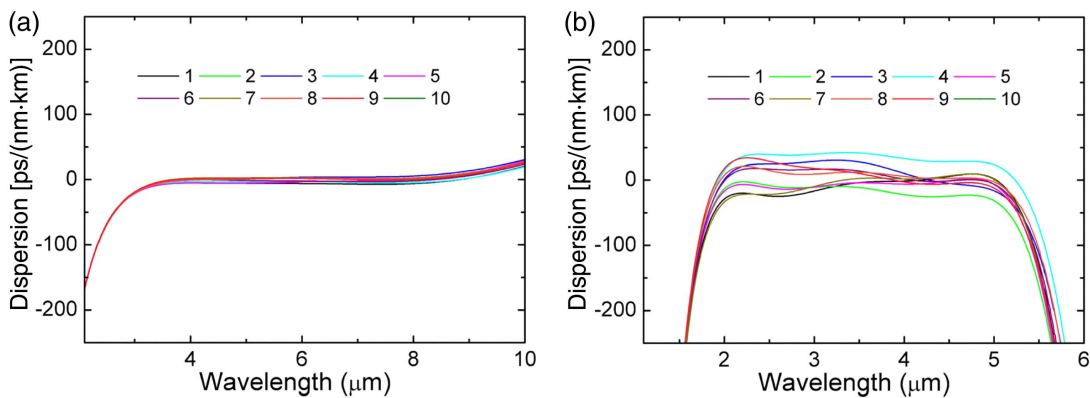

Fig. 5. Dispersion profiles of the waveguides with the six structural parameters randomly changed within a range of $\pm 2.5\%$ for 10 times to mimic the influence of fabrication errors (a) for WG1 and (b) for WG2.

Table 2. Values of the Six Structural Parameters Randomly Changed within a Range of ±2.5% for 10 Times for WG1 (unit: nm)

	1	2	3	4	5	6	7	8	9	10
W	2174	2185	2260	2184	2239	2087	2180	2155	2113	2228
H_1	727	728	717	723	711	735	695	728	704	713
H_2	469	453	436	440	448	459	435	423	434	454
H_3	2531	2521	2510	2550	2455	2647	2618	2583	2580	2533
H_4	724	720	696	740	726	714	720	715	690	715
H_5	2799	2720	2681	2822	2714	2689	2709	2672	2653	2902

Table 3. Values of the Six Structural Parameters Randomly Changed within a Range of ±2.5% for 10 Times for WG2 (unit: nm)

	1	2	3	4	5	6	7	8	9	10
W	889	849	870	869	860	859	880	895	864	870
H_1	248	247	247	249	245	244	249	246	240	242
H_2	49.7	49.1	48.1	48.9	49.4	48.3	48.5	51.2	50.2	49.5
H_3	626	638	653	664	636	647	626	646	650	638
H_4	850	861	896	871	845	853	847	875	850	856
H_5	578	570	591	589	568	588	581	581	573	579

4. ANALYSIS OF FABRICATION TOLERANCE

In order to examine the fabrication tolerance of the proposed waveguides, we randomly change the six structural parameters within a range of ±2.5% for both WG1 and WG2, which is repeated 10 times. We plot the obtained dispersion profiles in Fig. 5. The structural parameters are listed in Tables 2 and 3. As shown in Fig. 5(a), the overall dispersion variation for WG1 is smaller than 15 ps/(nm·km) for all 10 cases, and the dispersion slope has a negligible change over the low-dispersion bandwidth, meaning that dispersion of this waveguide is tolerant to the dimension variations in device fabrication. Compared to WG1, WG2 is a bit more sensitive to dimension variations and the overall dispersion variation is about ±40 ps/(nm·km).

A suggested fabrication process for the waveguide is shown in Fig. 6. We take WG1 as an example. First, using thermal evaporation, a blanket film of GeSbS is deposited on top of a CaF$_2$ wafer. Then, a negative lift-off photoresist is spin-coated with a thickness slightly greater than that required for the devices to be fabricated. Using a chrome-on-quartz photomask, a pattern is created in the negative photoresist by exposure with a contact aligner. The UV light crosslinks the photoresist so that, when the sample is immersed in a developer solution containing tetramethyl ammonium hydroxide (TMAH), the unexposed regions are washed away. This leaves a negative image of the ultimate pattern. Following lithography, three successive thermal evaporation steps are carried out to build a structure comprised of a thin layer of GeSbS sandwiched between two thicker layers of GeSbSe. As a final step, a thin layer of GeSbS is thermally evaporated to coat the devices. It is important to mention that waveguide sidewalls may not be maintained vertical after fabrication, and this can result in a change in the dispersion profile. However, it can be corrected by slightly tailoring other structural parameters.
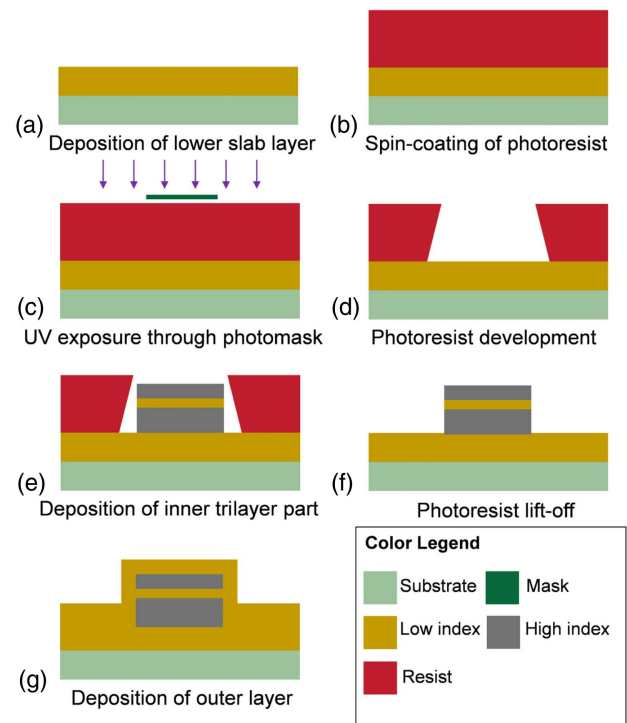

Fig. 6. Suggested waveguide fabrication process. (a) Thermal evaporation of GeSbS. (b) Spin-coating of photoresist. (c) UV exposure through photomask. (d) Photoresist development. (e) Thermal evaporation of GeSbSe, GeSbS, and GeSbSe. (f) Photoresist lift-off. (g) Thermal evaporation of GeSbS.

5. CONCLUSION AND OUTLOOK

In conclusion, we propose a new dispersion-flattening technology that generates an ultra-flat dispersion profile with five or even six ZDWs. Two material combinations with

different index contrasts are presented to realize dispersion flattening, exhibiting the universality of the proposed dispersion engineering scheme. A very small dispersion variation of 0.5 ps/(nm·km) can be obtained in the chalcogenide waveguide over a broad band more than one octave in the deep mid-IR. The dispersion flatness can be as large as 8000 nm² · km/ps, which is the highest to the best of our knowledge. The proposed silicon waveguide exhibits six ZDWs in a flattened dispersion profile, which has never been demonstrated in optical waveguides and fibers.

The dispersion-flattened waveguides in this work represent the unprecedented capability of dispersion engineering in high-index-contrast integrated photonics, which has not been shown in optical fibers. This proves that high-index-contrast waveguides are not only suitable for producing strong dispersion but are also feasible to enable ultra-small dispersion over a wide bandwidth. This greatly extends parameter space of dispersion engineering originating from optical fiber technologies. More importantly, generating five or even six ZDWs is expected to open an opportunity for exploring enriched nonlinear phenomena and mechanisms in broadband mid-IR photonics.

REFERENCES

1. G. P. Agrawal, *Nonlinear Fiber Optics*, 4th ed. (Academic, 2006).
2. M. Marhic, *Fiber Optical Parametric Amplifiers, Oscillators and Related Devices*, 1st ed. (Cambridge University, 2007).
3. R. R. Alfano, *The Supercontinuum Laser Source*, 1st ed. (Springer, 1989).
4. J. Ye and S. T. Cundiff, *Femtosecond Optical Frequency Comb: Principle, Operation, and Applications*, 1st ed. (Springer, 2004).
5. Y. Guo, J. Wang, Z. Han, K. Wada, L. C. Kimerling, A. M. Agarwal, J. Michel, Z. Zheng, G. Li, and L. Zhang, "Power-efficient generation of octave-spanning mid-IR frequency combs in a germanium," Nanophotonics **7**, 1461–1467 (2018).
6. C. R. Petersen, U. Møller, I. Kubat, B. Zhou, S. Dupont, J. Ramsay, T. Benson, S. Sujecki, N. Abdel-Moneim, Z. Tang, D. Furniss, A. Seddon, and O. Bang, "Mid-infrared supercontinuum covering the 1.4-13.3 μm molecular fingerprint region using ultra-high NA chalcogenide step-index fibre," Nat. Photonics **8**, 830–834 (2014).
7. M. Yang, L. Xu, J. Wang, H. Liu, X. Zhou, G. Li, and L. Zhang, "An octave-spanning optical parametric amplifier based on a low-dispersion silicon-rich nitride waveguide," IEEE J. Sel. Top. Quantum Electron. **24**, 8300607 (2018).
8. A. Ferrando, E. Silvestre, J. J. Miret, and P. Andrés, "Nearly zero ultra-flattened dispersion in photonic crystal fibers," Opt. Lett. **25**, 790–792 (2000).
9. F. Poletti, V. Finazzi, T. M. Monro, N. G. R. Broderick, V. Tse, and D. J. Richardson, "Inverse design and fabrication tolerances of ultra-flattened dispersion holey fibers," Opt. Express **13**, 3728–3736 (2005).
10. S. Kim, C. S. Kee, and J. Lee, "Novel optical properties of six-fold symmetric photonic quasicrystal fibers," Opt. Express **15**, 13221–13226 (2007).
11. D. J. J. Hu, P. P. Shum, C. Lu, and G. Ren, "Dispersion-flattened polarization-maintaining photonic crystal fiber for nonlinear applications," Opt. Commun. **282**, 4072–4076 (2009).
12. H. Xu, J. Wu, K. Xu, Y. Dai, C. Xu, and J. Lin, "Ultra-flattened chromatic dispersion control for circular photonic crystal fibers," J. Opt. **13**, 055405 (2011).
13. A. C. Turner, C. Manolatou, B. S. Schmidt, M. Lipson, M. A. Foster, J. E. Sharping, and A. L. Gaeta, "Tailored anomalous GVD in Si channel waveguides," Opt. Express **14**, 4357–4362 (2006).
14. L. Zhang, Y. Yan, Y. Yue, Q. Lin, O. Painter, R. G. Beausoleil, and A. E. Willner, "On-chip two-octave supercontinuum generation by enhancing self-steepening of optical pulses," Opt. Express **19**, 11584–11590 (2011).
15. L. Zhang, Q. Lin, Y. Yue, Y. Yan, R. G. Beausoleil, and A. E. Willner, "Silicon waveguide with four zero-dispersion wavelengths and its application in on-chip octave-spanning supercontinuum generation," Opt. Express **20**, 1685–1690 (2012).
16. H. Lee, T. Chen, J. Li, K. Y. Yang, S. Jeon, O. Painter, and K. J. Vahala, "Chemically etched ultrahigh-Q wedge-resonator on a silicon chip," Nat. Photonics **6**, 369–373 (2012).
17. Z. Jafari, L. Zhang, A. M. Agarwal, L. C. Kimerling, J. Michel, and A. Zarifkar, "Parameter space exploration in dispersion engineering of multilayer silicon waveguides from near-infrared to mid-infrared," J. Lightwave Technol. **34**, 3696–3702 (2016).
18. M. Zhu, H. Liu, X. Li, N. Huang, Q. Sun, J. Wen, and Z. Wang, "Ultrabroadband flat dispersion tailoring of dual-slot silicon waveguides," Opt. Express **20**, 15899–15907 (2012).
19. Z. Jafari and F. Emami, "Strip/slot hybrid arsenic tri-sulfide waveguide with ultra-flat and low dispersion profile over an ultra-wide bandwidth," Opt. Lett. **38**, 3082–3085 (2013).
20. D. Castelló-Lurbe, V. Torres-Company, and E. Silvestre, "Inverse dispersion engineering in silicon waveguides," J. Opt. Soc. Am. B **31**, 1829–1835 (2014).
21. Y. Zhang, H. Liu, Q. Sun, N. Huang, and Z. Wang, "Supercontinuum generation in strip/slot hybrid waveguide with flat and low dispersion," Appl. Opt. **54**, 4850–4856 (2015).
22. L. Xu, X. Ni, B. Liu, Y. Li, and M. Hu, "Ultraflat and low dispersion in a horizontal silicon nitride slot waveguide at near-infrared wavelengths," Opt. Eng. **55**, 037109 (2016).
23. R. H. Khandokar, M. Bakaul, S. Skafidas, T. Nirmalathas, and M. Asaduzzaman, "Performance of planar, rib and photonic crystal silicon waveguides in tailoring group-velocity dispersion and mode loss," IEEE J. Sel. Top. Quantum Electron. **22**, 73–80 (2016).
24. Y. Guo, Z. Jafari, A. M. Agarwal, L. C. Kimerling, G. Li, J. Michel, and L. Zhang, "Bilayer dispersion-flattened waveguides with four zero-dispersion wavelengths," Opt. Lett. **41**, 4939–4942 (2016).
25. A. D. Torre, M. Sinobad, B. Luther-Davis, P. Ma, S. Madden, S. Debbarma, K. Vu, D. J. Moss, A. Mitchell, J. Hartmann, J. Fedeli, C. Monat, and C. Grillet, "Tailoring the dispersion of a hybrid chalcogenide/silicon-germanium waveguide for mid-infrared supercontinuum generation," in *Conference on Lasers and Electro-Optics*, OSA Technical Digest (Optical Society of America, 2019), paper FF2D.8.
26. M. M. Borhan, J. Nafiz, and K. Sangsik, "Extremely high dispersions in heterogeneously coupled waveguides," Opt. Express **27**, 10426–10437 (2019).
27. B. J. Eggleton, B. L. Davies, and K. Richardson, "Chalcogenide photonics," Nat. Photonics **5**, 141–148 (2011).
28. R. Shankar and M. Lončar, "Silicon photonic devices for mid-infrared applications," Nanophotonics **3**, 329–341 (2014).
29. L. Zhang, A. M. Agarwal, L. C. Kimerling, and J. Michel, "Nonlinear group IV photonics based on silicon and germanium: from near-infrared to mid-infrared," Nanophotonics **3**, 247–268 (2014).
30. M. Li, L. Zhang, L. Tong, and D. Dai, "Hybrid silicon nonlinear photonics [Invited]," Photon. Res. **6**, B13–B22 (2018).
31. N. Singh, D. D. Hudson, Y. Yu, C. Grillet, S. D. Jackson, A. C. Bedoya, A. Read, P. Atanackovic, S. G. Duval, S. Palomba, B. L. Davies, S. Madden, D. J. Moss, and B. J. Eggleton, "Mid-infrared supercontinuum generation from 2 to 6 μm in a silicon nanowire," Optica **2**, 797–802 (2015).
32. M. Yang, Y. Guo, J. Wang, Z. Han, K. Wada, L. C. Kimerling, A. M. Agarwal, J. Michel, G. Li, and L. Zhang, "Mid-IR supercontinuum generated in low-dispersion Ge-on-Si waveguides pumped by sub-ps pulses," Opt. Express **25**, 16116–16122 (2017).

33. M. Sinobad, C. Monat, B. Luther-Davies, P. Ma, S. Madden, D. J. Moss, A. Mitchell, D. Allioux, R. Orobtchouk, S. Boutami, J. M. Hartmann, J. M. Fedeli, and C. Grillet, "Mid-infrared octave spanning supercontinuum generation to 8.5 μm in silicon-germanium wave-guides," Optica **5**, 360–366 (2018).

34. A. G. Griffith, R. K. W. Lau, J. Cardenas, Y. Okawachi, A. Mohanty, R. Fain, Y. H. D. Lee, M. Yu, C. T. Phare, C. B. Poitras, A. L. Gaeta, and M. Lipson, "Silicon-chip mid-infrared frequency comb generation," Nat. Commun. **6**, 6299 (2015).

35. A. A. Savchenkov, V. S. Ilchenko, F. Di Teodoro, P. M. Belden, W. T. Lotshaw, A. B. Matsko, and L. Maleki, "Generation of Kerr combs centered at 4.5 μm in crystalline microresonators pumped with quantum-cascade lasers," Opt. Lett. **40**, 3468–3471 (2015).

36. D. Benedikovic, L. Virot, G. Aubin, F. Amar, B. Szelag, B. Karakus, J. Hartmann, C. Alonso-Ramos, X. L. Roux, P. Crozat, E. Cassan, D. Marris-Morini, C. Baudot, F. Boeuf, J. Fédéli, C. Kopp, and L. Vivien, "25 Gbps low-voltage hetero-structured silicon-germanium waveguide pin photodetectors for monolithic on-chip nanophotonic architectures," Photon. Res. **7**, 437–444 (2019).

37. J. G. Crowder, S. D. Smith, A. Vass, and J. Keddie, "Infrared methods for gas detection," in *Mid-Infrared Semiconductor Optoelectronics* (Springer, 2006), pp. 595–613.

38. S. Türker-Kaya and C. W. Huck, "A review of mid-infrared and near-infrared imaging: principles concepts and applications in plant tissue analysis," Molecules **22**, 168 (2017).

39. J. M. Ramirez, V. Vakarin, J. Frigerio, P. Chaisakul, D. Chrastina, X. Le Roux, A. Ballabio, L. Vivien, G. Isella, and D. Marris-Morini, "Ge-rich graded-index Si$_{1-x}$Ge$_x$ waveguides with broadband tight mode confinement and flat anomalous dispersion for nonlinear mid-infrared photonics," Opt. Express **25**, 6561–6567 (2017).

40. J. Yuan, Z. Kang, F. Li, X. Zhang, X. Sang, Q. Wu, B. Yan, K. Wang, X. Zhou, K. Zhong, G. Zhou, C. Yu, C. Lu, H. Y. Tam, and P. K. A. Wai, "Mid-infrared octave-spanning supercontinuum and frequency comb generation in a suspended germanium-membrane ridge wave-guide," J. Lightwave Technol. **35**, 2994–3002 (2017).

41. Z. Cheng, X. Chen, C. Y. Wong, K. Xu, C. K. Y. Fung, Y. M. Chen, and H. K. Tsang, "Broadband focusing grating couplers for suspended-membrane waveguides," Opt. Lett. **37**, 5181–5183 (2012).

42. H. H. Li, "Refractive index of alkaline earth halides and its wavelength and temperature derivatives," J. Phys. Chem. Ref. Data **9**, 161–289 (1980).

43. E. D. Palik, ed., *Handbook of Optical Constants of Solids I* (Academic, 1985).

44. K. Luke, Y. Okawachi, M. R. E. Lamont, A. L. Gaeta, and M. Lipson, "Broadband mid-infrared frequency comb generation in a Si$_3$N$_4$ micro-resonator," Opt. Lett. **40**, 4823–4826 (2015).

45. Q. Lin, O. J. Painter, and G. P. Agrawal, "Nonlinear optical phenomena in silicon waveguides: modeling and applications," Opt. Express **15**, 16604–16644 (2007).

46. A. W. Synder, "Excitation and scattering of modes on a dielectric or optical fiber," IEEE Trans. Microwave Theory Tech. **17**, 1138–1144 (1969).